Transverse Anisotropy Stabilizes Concentric Tube Robots

Caleb Rucker *Member, IEEE*, Jake Childs *Student Member, IEEE*,
Parsa Molaei *Student Member, IEEE*, Hunter B. Gilbert *Member, IEEE*,

***Abstract*—We propose a new method for improving the stability of concentric tube robots. Prior work sought to improve stability through laser-cut patterns that reduced EI/GJ, the ratio of flexural rigidity to torsional rigidity, but this strategy has always entailed a steep trade-off in overall robot stiffness. Instead, we show that stability can be improved much more efficiently by allowing transverse anisotropy (direction-dependent flexural rigidity, $EI_x \neq EI_y$). We provide a generalized robot model with this property and give its associated stability criterion. In the two-tube case, this provides a new version of the well-known EI/GJ criterion, now generalized to reveal the independent effects of EI_x and EI_y. It shows that the most efficient strategy to improve stability while preserving stiffness is to reduce the flexural rigidity about the axis of precurvature while maintaining high off-axis flexural rigidity and torsional rigidity. We validate the approach with a balanced-stiffness pair of laser-machined Nitinol tubes, demonstrating model accuracy and significant stability improvement while requiring less stiffness reduction than prior methods.**

***Index Terms*—Surgical Robot, Continuum Robot, Elastic Stability**

I. Introduction

Concentric-tube robots (CTRs) are slender manipulators composed of two or more precurved elastic tubes nested together. Axial rotations and translations of the tube bases by actuators cause the tubes to bend and twist one another, which changes the shape of the collection and moves the tip through space. This creates a highly miniaturizable device that is potentially useful in minimally invasive surgical applications to navigate through tight spaces and deliver therapy [1].

Ever since their initial introduction, the *elastic stability* of concentric tube robots has been a rich topic of research and discussion. As first identified in [2], a so-called "snapping" instability can happen when two tubes with overlapping curved regions are rotated with respect to each other. The tubes reach a point where much of the stored elastic energy suddenly releases, and the tubes "snap" to a new configuration with high velocity. The existence of such unstable events limits the robot's workspace and implies the existence of multiple solutions to the forward kinematics problem [3], [4], thus complicating modeling and control. The theory and understanding of CTR stability was expanded in [5]–[8] which also developed numerical tests to determine if particular configurations and designs will be stable. The dynamics of the unstable transitions were recently modeled in [9].

Though some have proposed ways to harness the snapping transitions for useful purposes [10], much recent CTR research has focused on avoiding unstable behavior by planning and controlling the robot to follow stable actuation trajectories [5], [11]–[16], or by designing the tube precurvatures and overlap regions such that instabilities do not exist in the configuration space [8], [17]–[21].

A. Stability through Structural Modification

In the development of the now standard CTR mechanics model [3], [4], [22] and its analytical solution in the two-tube case, the authors found the inequality

$$L^2 c < \frac{\pi^2}{4} \tag{1}$$

to be necessary and sufficient for the stability of the entire rotation space of two tubes with constant precurvature, where L is the overlapped length,

$$c = \kappa_1 \kappa_2 \frac{EI_1 EI_2 (GJ_1 + GJ_2)}{(EI_1 + EI_2) GJ_1 GJ_2} \tag{2}$$

and EI_i, GJ_i, and κ_i are the flexural rigidity, torsional rigidity, and precurvature of the i^{th} tube. If the two tubes have identical stiffnesses and precurvatures (a usually impractical case, but useful for gaining insight) then the stability condition reduces to

$$(\kappa L)^2 \frac{EI}{GJ} < \frac{\pi^2}{4} \tag{3}$$

This observation inspired further research on potential ways to reduce the effective ratio of flexural rigidity EI to torsional rigidity GJ for a given tube, so that robots could be made capable of greater bending angles (κL) while remaining stable over the whole rotation space. In [23]–[26], patterns of horizontal slots were laser cut into the tube walls. Typical results from these studies showed that the strategy was able to reduce the effective EI/GJ to 0.4 (29% of its original value of 1.3), but this required reduction in EI itself to around 3% of its original value. In [27], topology optimization was used to identify a pattern of holes that reduced EI/GJ to 1.0, (77% of 1.3), but this reduced EI itself to 47% of its original value. In

Manuscript received: September 9, 2021; Revised: November 24, 2021; Accepted: December 22, 2021. This paper was recommended for publication by Editor Pietro Valdastri upon evaluation of the Associate Editor and Reviewers' comments. This work was supported by the National Science Foundation under CAREER Award IIS-1652588. Any opinion, findings, and conclusions or recommendations expressed in this material are those of the authors and do not necessarily reflect the views of the National Science Foundation.

Caleb Rucker and Jake Childs are with the University of Tennessee, Knoxville, TN 37996, USA caleb.rucker@utk.edu. Parsa Molaei and Hunter Gilbert are with the Louisiana State University, Baton Rouge, 70803 USA. Digital Object Identifier (DOI): see top of this page.

[28], 3D printed bellows tubes were used to create larger soft robot segments with very low EI/GJ ratios around 0.05, but also with extremely low bending stiffness considering the tube diameter. Recently, [29], [30] studied auxetic cutting patterns in tubes and showed that the bending and torsional stiffnesses are independently controllable. However, the boundary of the feasible parameter space shown in Figure 6 of [30] again reveals the fundamental tradeoff: reducing EI/GJ by 50% would require a reduction in EI by about 80% or more.

B. Contributions

The above results demonstrate that the main trade-off inherent to structural modification thus far has been the drastic reduction in bending stiffness required to achieve sufficient stability improvement, which consequently weakens the robot's capacity to apply or resist forces. Our contribution in this paper is a new approach to CTR stability improvement in which this trade-off is far less severe. The strategy we propose is to endow the tubes with direction-dependent flexural rigidity ($EI_x \neq EI_y$), creating what is known as a "transversely anisotropic" member [31]. As shown in Figure 1, we propose a cut pattern that reduces the flexural rigidity about one axis (the axis of precurvature) more than the other. Direction-dependent flexural rigidity has been a feature of other robots for various purposes [32]–[35], but no research has yet investigated the effect of such transverse anisotropy on the stability of precurved concentric tube robots.

To fill this gap, we first present the standard CTR model [22] in a generalized form that accommodates transverse anisotropy. Using this model, we examine the stability of the two-tube case, generalizing the prior stability condition (3) to reveal the independent effects of EI_x and EI_y and the benefits of direction-dependent rigidity. We further explore the improved stiffness/stability trade-off through characteristic input-output angle curves, and comparisons to existing designs from the literature (see Figure 4). Finally, we provide a realistic example using a pair of transversely anisotropic laser-cut tubes, and validate the stability predictions experimentally.

II. Mechanics Model with Transverse Anisotropy

In this section we provide a short summary of the equations of the standard CTR mechanics model with external loading, but without applying the typical assumption that $EI_x = EI_y$. Each tube in a CTR obeys the static equilibrium conditions for a Cosserat rod [31]:

$$\begin{aligned} \dot{\mathbf{n}}_i + \mathbf{f}_i &= 0 \\ \dot{\mathbf{m}}_i + \dot{\mathbf{p}}_i \times \mathbf{n}_i + \mathbf{l}_i &= 0 \end{aligned} \tag{4}$$

and the kinematic equations

$$\begin{aligned} \dot{\mathbf{p}}_i &= \mathbf{R}_i \mathbf{e}_3 \\ \dot{\mathbf{R}}_i &= \mathbf{R}_i \widehat{\mathbf{u}}_i \end{aligned} \tag{5}$$

where the subscript i denotes the tube index, $\mathbf{m}_i : \mathbb{R} \mapsto \mathbb{R}^3$ is the tube's internal moment, $\mathbf{l}_i : \mathbb{R} \mapsto \mathbb{R}^3$ is an external distributed moment, $\mathbf{n}_i : \mathbb{R} \mapsto \mathbb{R}^3$ is the internal force, $\mathbf{f}_i : \mathbb{R} \mapsto \mathbb{R}^3$ is an external distributed force $\mathbf{p}_i : \mathbb{R} \mapsto \mathbb{R}^3$ is the position, $\mathbf{R}_i : \mathbb{R} \mapsto \mathrm{SO}(3)$ is the orientation, $\mathbf{u}_i : \mathbb{R} \mapsto \mathbb{R}^3$ is the curvature vector, and $\mathbf{e}_3 = [0 \;\; 0 \;\; 1]^\top$. All variables are functions of the reference arc length $s \in [0 \;\; L]$ along the tube centerline. The $\dot{}$ denotes a derivative with respect to s, and $\widehat{}\, : \mathbb{R}^3 \mapsto \mathfrak{so}(3)$ denotes the standard skew-symmetric form of a vector [36].

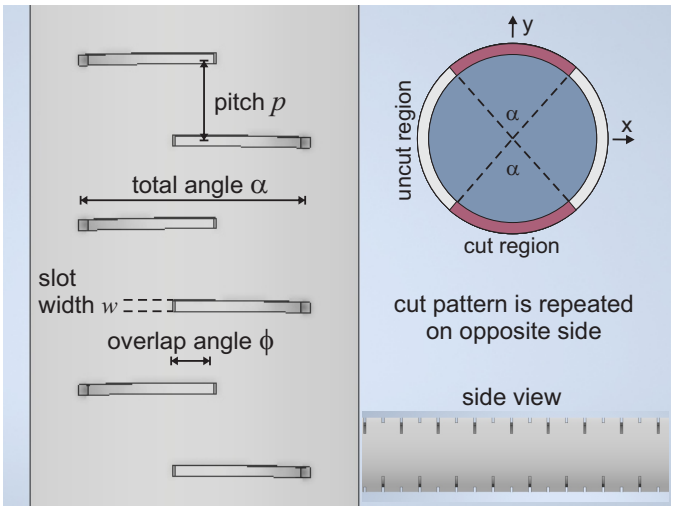

Figure 1. If the tube is precurved locally about the x-axis, we propose to lower the flexural rigidity EI_x relative to the off-axis flexural rigidity EI_y and the torsional rigidity GJ. To accomplish this, the cut pattern shown above is used in our prototype design.

A linear constitutive law relates the kinematics to the statics as

$$\mathbf{m}_i = \mathbf{R}_i \mathbf{K}_i (\mathbf{u}_i - \mathbf{u}_i^*)$$

where $\mathbf{K}_i = \mathrm{diag}(EI_{xi}, EI_{yi}, GJ_i)$ and $\widehat{\mathbf{u}}_i^* = \mathbf{R}_i^{*\top} \dot{\mathbf{R}}_i^*$ is the precurvature vector in the unstressed state ($\mathbf{R}_i^*$ is the rotation matrix assigned in the unstressed state).[1] We can differentiate the constitutive law and substitute into (4). We then multiply by $\mathbf{e}_3^\top \mathbf{R}_i^\top$ and solve for $\dot{u}_{iz}$ as:

$$\dot{u}_{iz} = \dot{u}_{iz}^* - \frac{1}{GJ_i} \mathbf{e}_3^\top (\widehat{\mathbf{u}}_i \mathbf{K}_i + \dot{\mathbf{K}}_i)(\mathbf{u}_i - \mathbf{u}_i^*) \tag{6}$$

where $\mathbf{e}_3^\top \mathbf{R}_i^\top \mathbf{l}_i = 0$ under the assumption of no torsional friction, and $\mathbf{e}_3^\top \mathbf{R}_i^\top (\dot{\mathbf{p}}_i \times \mathbf{n}_i) = 0$ identically because of (5). Note that (6) was simplified in all prior work by assuming $EI_x = EI_y$, but we are intentionally not making that assumption here, so we leave (6) in its general form.

The x and y components of the tube curvature $\mathbf{u}_i$ can be related to the curvature $\mathbf{u} = [u_x \;\; u_y \;\; 0]^\top$ of a Bishop frame $\mathbf{R}$ that slides along the robot centerline with no torsion:

$$\dot{\mathbf{R}} = \mathbf{R}\widehat{\mathbf{u}} \quad \dot{\mathbf{p}} = \mathbf{R}\mathbf{e}_3 \tag{7}$$

Based on the concentric constraint $\dot{\mathbf{p}}_i = \dot{\mathbf{p}}$, we have

$$\mathbf{R}_i = \mathbf{R} \begin{bmatrix} \cos\psi_i & -\sin\psi_i & 0 \\ \sin\psi_i & \cos\psi_i & 0 \\ 0 & 0 & 1 \end{bmatrix} = \mathbf{R} \begin{bmatrix} \mathbf{R}_{\psi_i} & 0_{2\times 1} \\ 0_{1\times 2} & 1 \end{bmatrix}, \tag{8}$$

[1]Note that we can assume $\mathbf{K}_i$ is diagonal without loss of generalization because we can always assign the initial reference frame $\mathbf{R}_i^*(s)$ such that the x and y axes align with the effective principal axes at s. This can be done even if the principal axes vary along the length, which would simply entail $\mathbf{u}_i^*(s)$ having a nonzero torsional component, as in [37].

And the curvature relationship is then

$$\begin{bmatrix} u_{ix} \\ u_{iy} \end{bmatrix} = \mathbf{R}_{\psi_i}^{\top} \begin{bmatrix} u_x \\ u_y \end{bmatrix} \tag{9}$$

where

$$\dot{\psi}_i = u_{iz} \tag{10}$$

Enforcing the concentric constraint $\dot{\mathbf{p}}_i = \dot{\mathbf{p}} \ \ \forall i$, and defining $\mathbf{m} = \sum_{i=1}^{n} \mathbf{m}_i$, $\mathbf{n} = \sum_{i=1}^{n} \mathbf{n}_i$, and $\mathbf{f} = \sum_{i=1}^{n} \mathbf{f}_i$ we have

$$\begin{aligned} \dot{\mathbf{n}} + \mathbf{f} &= 0 \\ \dot{\mathbf{m}} + \dot{\mathbf{p}} \times \mathbf{n} + \mathbf{l} &= 0 \end{aligned} \tag{11}$$

and from the above definitions we can algebraically derive

$$\mathbf{u}_{xy} = \left(\sum_{i=1}^{n} \mathbf{R}_{\psi_i} \mathbf{K}_{bi} \mathbf{R}_{\psi_i}^{\top} \right)^{-1} \left(\sum_{i=1}^{n} \mathbf{R}_{\psi_i} \mathbf{K}_{bi} \mathbf{u}_i^{*} + \begin{bmatrix} m_x \\ m_y \end{bmatrix} \right) \tag{12}$$

where $\mathbf{K}_{bi} = \text{diag}(EI_{xi}, EI_{yi})$, and m_x and m_y are the x and y components of $\mathbf{m}$ expressed in the Bishop frame $\mathbf{R}$, i.e. $[m_x \ \ m_y \ \ m_z]^{\top} = \mathbf{R}^{\top}\mathbf{m}$

Thus Equations 6, 7, 10, and 11 provide a complete set of differential equations for the robot state variables with Equations 8, 9, and 12 providing the algebraic relationships to compute necessary quantities and other variables of interest. Boundary conditions of a concentric tube system are detailed in many prior publications [3], [4]. These usually specify the proximal angle of each tube $\psi_i(\beta_i)$ (where β_i is the arc length at which tube i is held by the rotary actuator), and the distal torsion at the free end ($u_{iz}(\ell_i) = 0$ if tube i ends at $s = \ell_i$).

The stability of a given solution to the above general boundary value problem can be evaluated using the method of [7] based on a criterion adapted from optimal control, namely the "conjugate-point test". In the unloaded case, this is equivalent to the criteria of [8]. In the subsequent development in this paper, we will consider the unloaded scenario, and specifically the two-tube case in order to gain practical insight into the design of stable tube pairs.

III. Two Tubes with Transverse Anisotropy

In this section we will examine the case of two tubes with constant $\mathbf{K}_i$ and uniform precurvatures κ_1 and κ_2 about their x axes ($\mathbf{u}_i^{*} = [\kappa_i \ 0 \ 0]^{\top}$). In this case (6) reduces to

$$\dot{u}_{iz} = \frac{1}{GJ_i} \left((EI_{ix} - EI_{iy}) u_{ix} u_{iy} - EI_{ix} \kappa_i u_{iy} \right) \tag{13}$$

and the differential equation governing the relative tube angle $\theta = \psi_2 - \psi_1$ can then be expressed as

$$\ddot{\theta} = \boldsymbol{\kappa}^{\top} \mathbf{A}(\theta) \boldsymbol{\kappa} \sin\theta \tag{14}$$

where $\boldsymbol{\kappa} = [\kappa_1 \quad \kappa_2]^{\top}$, and the matrix $\mathbf{A}(\theta)$ is given by

$$\mathbf{A}(\theta) = \frac{(\gamma_1 + \gamma_2) \begin{bmatrix} \chi_1\chi_2 + \chi_1\gamma_1 \\ (\chi_2\gamma_1 - \chi_1\chi_2)C_\theta \end{bmatrix} \begin{bmatrix} (\chi_1\gamma_2 - \chi_1\chi_2)C_\theta \\ \chi_1\chi_2 + \chi_2\gamma_2 \end{bmatrix}^{\top}}{\frac{\mu_1\mu_2}{\mu_1 + \mu_2} \begin{vmatrix} \chi_1 + \gamma_2 & (\chi_1 - \gamma_1)C_\theta \\ (\chi_2 - \gamma_2)C_\theta & \chi_2 + \gamma_1 \end{vmatrix}^2}$$

where $C_\theta = \cos\theta$, and we have defined the following symbols for notational compactness:

$$\chi_i = EI_{ix} \qquad \gamma_i = EI_{iy} \qquad \mu_i = GJ_i \tag{15}$$

The boundary conditions of (14) are $\theta(0) = \theta_0$, and $\dot{\theta}(L) = 0$. $\theta(L)$ is denoted by θ_L.

A. General Two-Tube Stability Criterion

We can evaluate the stability of a particular configuration by computing the solution $h(s)$ of the variational equation along any solution curve $\theta(s)$, which is an established stability metric [8]. The function $h(s)$ is associated with a solution $\theta(s)$ as follows:

$$\begin{aligned} \ddot{h}(s) &= \frac{\partial}{\partial\alpha} \left\{ \boldsymbol{\kappa}^{\top} \mathbf{A}(\alpha) \boldsymbol{\kappa} \sin\alpha \right\}_{\alpha=\theta(s)} h(s) \\ h(L) &= 1 \\ \dot{h}(L) &= 0 \end{aligned} \tag{16}$$

The solution $\theta(s)$ is stable if and only if the associated $h(s)$ satisfies

$$h(s) > 0 \ \ \forall s \in [0 \ \ L] \tag{17}$$

(i.e., there are no conjugate points [7], [38]). Physically, this condition means that positive variations in the angle at the distal end of the robot correspond only to positive variations in angle along the entire length of the robot. Graphically, $h(0) = \frac{d\theta_0}{d\theta_L}$ is the inverse of the slope of the curve at a point (θ_0, θ_L) on the locus of static equilibria as shown in Figures 2 and 3. And energetically, if the condition holds, the system energy is locally positive definite around the static equilibrium with regard to variations in $\theta(s)$.

In the general case, analytical solutions to (14) and (16) are not available, so no closed-form stability condition can be found. However, for any numerically evaluated solution $\theta(s)$, we can evaluate the stability criteria numerically, and we can test whether the entire rotation space is stable by sampling $\theta_L \in [0 \ 2\pi]^{\top}$ with sufficient resolution.

B. Stability of the Stationary Solution $\theta(s) = \pi$

Note that $\theta(s) = \pi$ is a stationary solution to (14). Intuitively, this solution is important to analyze because, in the case of transversely isotropic (symmetric) tubes, it is the first configuration to become unstable as the overlapped bending angle increases. It also admits a tractable solution and insight into the stability of the transversely anisotropic case. Applying (16) gives

$$\ddot{h} = -\boldsymbol{\kappa}^{\top} \mathbf{A}(\pi) \boldsymbol{\kappa} h = -Ch \tag{18}$$

where

$$\mathbf{A}(\pi) = \frac{(\mu_1 + \mu_2) \begin{bmatrix} \chi_1\chi_2 + \chi_1\gamma_1 \\ \chi_1\chi_2 - \chi_2\gamma_1 \end{bmatrix} \begin{bmatrix} \chi_1\chi_2 - \chi_1\gamma_2 \\ \chi_1\chi_2 + \chi_2\gamma_2 \end{bmatrix}^{\top}}{\mu_1\mu_2(\chi_1 + \chi_2)^2(\gamma_1 + \gamma_2)} \tag{19}$$

Thus the scalar constant $C = \boldsymbol{\kappa}^{\top} \mathbf{A}(\pi) \boldsymbol{\kappa}$ is a generalization of the constant c in [4], or a in [3], extended to the transversely anisotropic case. The conjugate point stability condition then gives

$$L^2 C < \frac{\pi^2}{4} \tag{20}$$

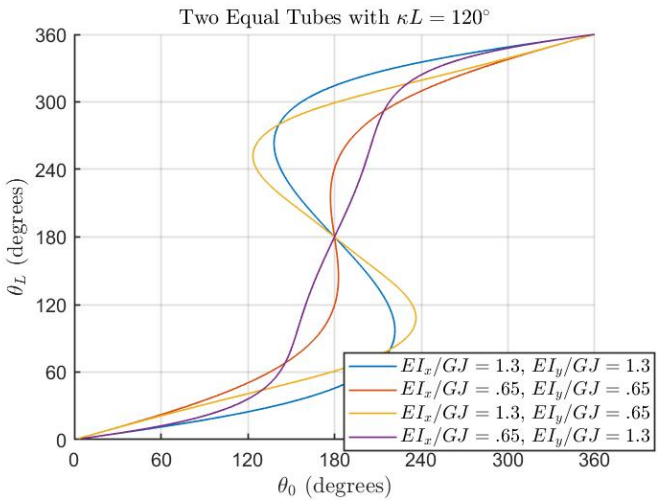

Figure 2. Input-output angle curves are shown for a two-tube robot with both tubes precurved about the x-axis to a 120° bending angle. The effect of various changes to EI_x and EI_y are shown while holding GJ constant. Reducing EI_x while preserving EI_y and GJ as much as possible is shown to be the best strategy.

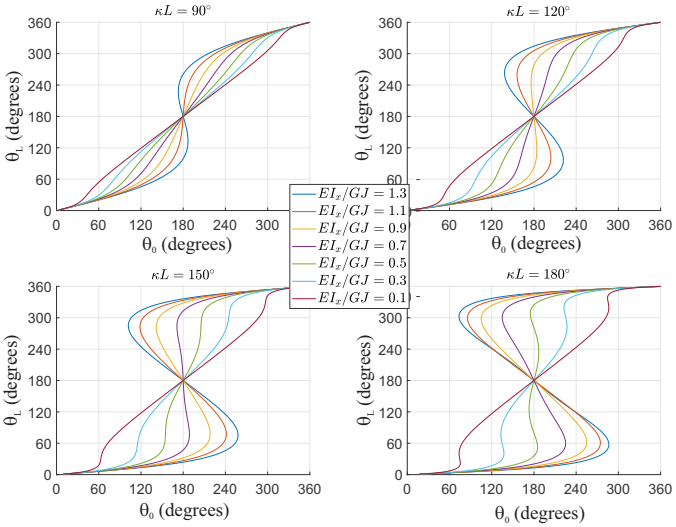

Figure 3. Input-output angle curves are shown for a two-tube robot with equal tubes having $EI_y/GJ = 1.3$. The effect of reducing only EI_x is shown for four different cases of bending angle κL. The plots illustrate that while the strategy is very effective at improving stability for tubes with moderate bending angles, it is not as effective for very large κL, because instabilities arise away from $\theta(s) = 180^\circ$. In these extreme cases, additional reduction in EI_y/GJ would stabilize the robot.

Of course, in the case of isotropic flexural rigidity, this condition reduces to the prior result (1).

C. A Simplified Stability Criteria for Design

If we examine the idealized case of two tubes with identical rigidities EI_x, EI_y, GJ, and precurvatures κ then (14) reduces to

$$\ddot{\theta} = \frac{4(EI_x)^2 EI_y \kappa^2 \sin\theta}{GJ(EI_x + EI_y + (EI_x - EI_y)\cos\theta)^2} \tag{21}$$

and (20) reduces to

$$L^2\kappa^2 \left(\frac{EI_x}{GJ}\right)\left(\frac{EI_x}{EI_y}\right) < \frac{\pi^2}{4} \tag{22}$$

This simple result provides a more complete understanding of stability than the well-established condition (3). Considering the conventional strategy of reducing EI/GJ, (22) reveals that reducing $(EI_x)^2/(GJEI_y)$ is a better objective. Although this expression reduces to EI/GJ in the isotropic (symmetric) case, it reveals that only the EI_x reduction improves the stability, and, contrary to current CTR knowledge and practice, reducing EI_y actually worsens the stability. We see that decreasing the flexural rigidity ratio EI_x/EI_y improves stability, making the left hand side of (22) proportional to $(EI_x)^2$. Thus (22) suggests we should attempt to reduce EI_x alone while preserving both EI_y and GJ as much as possible for robot strength. Additional advantages of this strategy include that (1) attempting to reduce only EI_x also makes it easier to preserve GJ, and (2) preserving EI_y also gives the robot higher out-of-plane stiffness.

In practice, the various reductions in EI_x, EI_y, and GJ will be coupled and dependent on the pattern of removed material, and the tubes may not have identical rigidities and curvatures. Thus, we will only use the simple result (22) as a heuristic to evaluate and improve the design of a single tube's material removal pattern, while using the exact general conditions (20) and (17) to formally evaluate the stability of a tube pair.

D. Stability Over the Rotation Space

To further illustrate the proposed strategy, the plots in Figure 2 show the conventional input-to-output angle mapping (θ_L vs. θ_0) for four different two-tube robot designs with two tubes having equal lengths, precurvatures, and rigidities, by solving (14) with $\dot{\theta}(L) = 0$. The precurvatures of the tubes are such that the total bending angle $\kappa L = 120^\circ$ when the tubes are aligned (an extreme case). The nominal case (blue line) has tubes with isotropic flexural rigidity and $EI/GJ = 1.3$, which is consistent with solid tube walls and a Poisson's ratio of $\nu = 0.3$. As discussed at length in [8], the regions of the plot with a negative value of $h = \frac{d\theta_0}{d\theta_L}$ (the reciprocal of the slope of the graph) represent unstable configurations, and the minimum value of h over the whole curve is a metric for stability of the configuration space. The value of L^2c in the nominal unmodified tube case is about 2.3 times larger than the maximum value for a stable configuration space, $\pi^2/4$. The red curve shows that an "almost stable" workspace can be achieved by reducing EI/GJ uniformly to half its previous value, but the instability around $\theta = \pi$ remains, and it is difficult to achieve such a reduction without dramatically reducing the overall flexural rigidity. The yellow curve shows that reducing EI_y/GJ alone actually makes the instability worse than the nominal case. Finally, the purple curve shows that reducing EI_x/GJ alone improves stability even more than the same amount of uniform reduction, while also preserving more of the original stiffness.

E. Extreme Cases

The previous sections analyzed the stability of the $\theta(s) = \pi$ configuration, and qualitatively examined the entire rotation space in an example case. The analysis clearly illustrates that reducing bending stiffness in only one direction (about

Table I
MODIFIED TUBE DESIGN PARAMETERS

	OD (mm)	ID (mm)	κ (1/m)	w (mm)	p (mm)	α (deg)	ϕ (deg)
Tube 1	3.00	2.76	14.0	0.1	0.75	89°	15°
Tube 2	2.54	2.20	13.5	0.1	0.75	85°	12°

the axis of precurvature) is a superior strategy for improving stability of the significant $\theta(s) = \pi$ configuration, but the question remains whether other configurations could ever become unstable due to the anisotropy itself.

The answer is yes, but only for extremely long or curved robots. Figure 3 illustrates this phenomenon for a pair of equal tubes with constant EI_y/GJ over a range of stiffness ratios EI_x/EI_y. The plots show that for a total bending angle less than about 150°, the tube pair can be stabilized by reducing EI_x alone, and stability of the $\theta = 180°$ configuration implies stability of the entire rotation space. However, the bottom plots show that for larger bending angles, instabilities (negative slope regions) are possible at other configurations even when $\theta(s) = 180°$ is stable. Thus, the minimum value of $\frac{d\theta_0}{d\theta_L}$ over the whole input-output curve should be used as a the stability metric in such cases. Studying how this value varies with changes in EI_y and EI_y would reveal the most efficient way to improve the stability for a given extreme design. In any case, stability of all points in the rotation space can be achieved by some combination of EI_x and EI_y reduction. But in the most practical cases, stability improvement can be most efficiently gained by reducing EI_x, relative to both EI_y and GJ, as shown by the top two plots.

The simulations in this section all used two equal tubes for simplicity and to build intuition in a reduced parameter space. For realistic CTRs, the tubes will likely be unequal, and full stability assessment will have to be done according to the general model we presented. However, the basic intuition gained by the comparisons in this section is still valid for unequal tubes, and we can further use the cut pattern to design certain properties to be equal if desired, as we show in the next section.

IV. EXPERIMENTAL VALIDATION

In the remainder of the paper, we investigate the benefits of transverse anisotropy in a prototype two-tube CTR segment.

A. Prototype Design

We selected two Nitinol tubes with parameters given in Table I. Our design goal was to significantly improve the workspace stability while preserving the strength of a tube pair with a curved length of $L = 100\ mm$ and $\mathbf{u}_1 = \mathbf{u}_2 = [\kappa \quad 0 \quad 0]^\top$, where the precurvature κ is such that the total bending angle is approximately 90°. We also aimed to produce tubes with equal EI_x so that the tube pair would be balanced and thus able to fully straighten.

We chose the pattern shown in Figure 1 because FEA simulations showed it was able to efficiently lower EI_x while preserving a significant portion of the original EI_y and GJ. We manually iterated the design parameters and performed finite element analysis to determine the effective flexural and torsional rigidities of 43 candidate designs. The resulting blue datapoints are plotted in Figure 4 showing the nondimensional relationship between $EI_x/EI_{x,solid}$ and our generalized stability parameter $(EI_x)^2/(GJEI_y)$ (lower is more stable). Figure 4 also shows in red a representative sampling of results obtained from prior published work [23], [25]–[27], [30] which sought to reduce EI/GJ by reducing EI in an isotropic (symmetric) manner. For isotropic designs, a theoretical performance bound can be obtained as $EI/GJ \geq EI/GJ_{solid}$, since GJ cannot be increased by removing material. In contrast, the performance of transversely

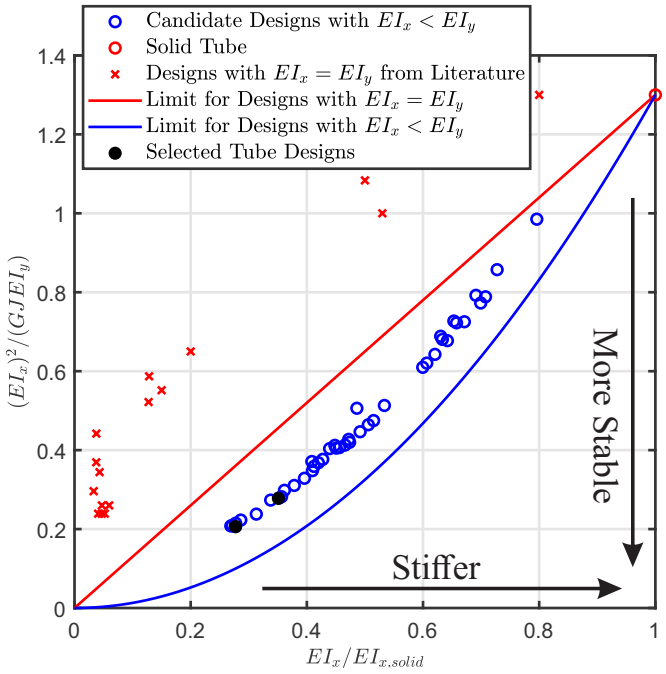

Figure 4. The relationship of flexural rigidity (stiffer toward the right) to stability (more stable toward the bottom) is depicted for 43 candidate transversely anisotropic designs simulated with finite element analysis (blue circles). All of the candidate designs were more ideal than prior designs with $EI_x = EI_y$ gathered from the literature (red x's) [23], [25]–[27], [30]. All candidates exceeded the theoretical performance bound for symmetric designs (red line) and came close to the bound for transversely anisotropic designs (blue line).

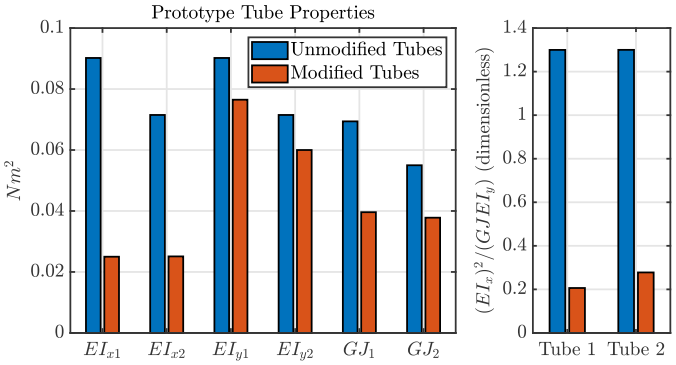

Figure 5. Rigidities and stability parameters of the unmodified and modified tubes are shown, as calculated from finite-element simulations.

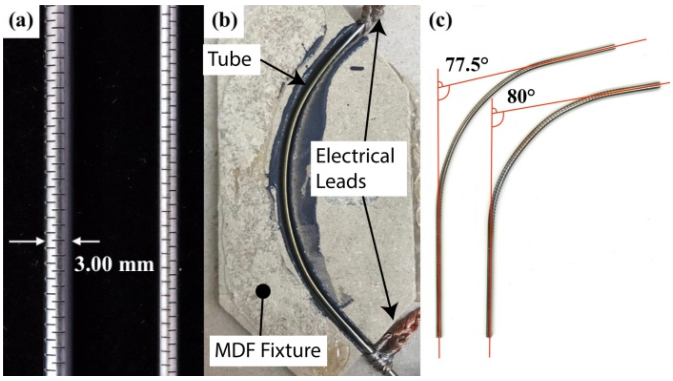

Figure 6. The manufacturing process, beginning with laser machining of the tubes, followed by shape setting and characterization.

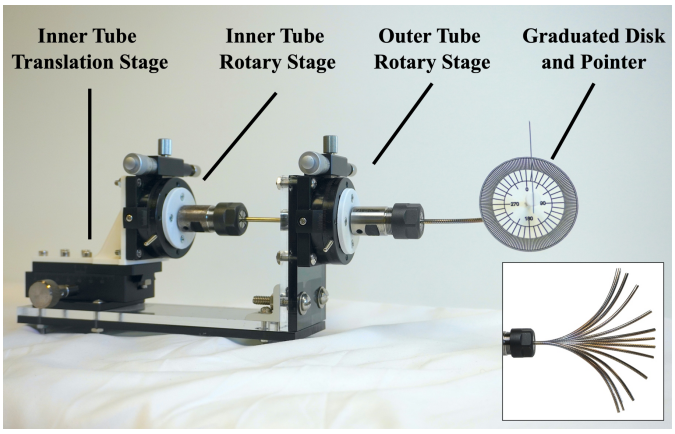

Figure 7. Manual actuation setup used to determine the experimental input-output angles. Inset figure shows the experimental range of motion of the modified tube pair.

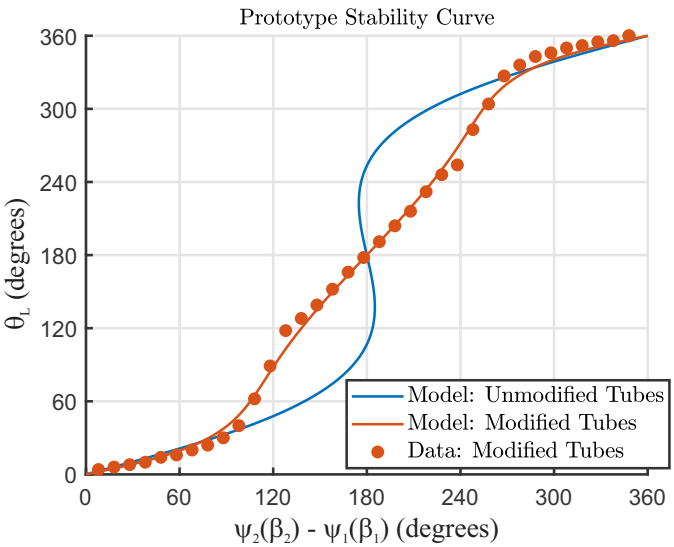

Figure 8. The experimental input-output angles are shown with the model prediction.

anisotropic designs is only bounded by $(EI_x)^2/(GJEI_y) \geq (EI_x)^2/(GJ_{solid}EI_{y,solid})$. These performance bounds are depicted by the red and blue lines in Figure 4. Note that stability of every transversely anisotropic design we tested was better than the theoretical performance bound for symmetric designs and came close to the bound for anisotropic designs. Note also that Figure 4 is conservatively plotted with the weaker rigidity on the horizontal axis. The overall stiffness of a given anisotropic design is even larger due to the minimal reduction in EI_y.

We eventually selected the design parameters given in Table I for each tube to satisfy our design goals. The resulting properties of the modified and unmodified tubes are depicted in Figure 5. Note that the modified EI_x of both tubes are equal, and EI_y and GJ have retained much of their original stiffness. Note that $(EI_x)^2/(GJEI_y)$ is reduced by a larger percentage than any of the individual stiffness reductions.

We cut the chosen pattern into straight, superelastic NiTi tubes using a pulsed fiber laser system. The resulting tubes are shown in Figure 6(a). The tubes were shape set via the resistance heating method described in [39] with a jig to enforce the desired curvature, as shown in Figure 6(b). The fixture was made of medium density fiberboard and coated in high temperature epoxy (J-B Kwik) to reduce charring. The electrical shape setting system was set to ramp the resistance of the part from its room temperature value R_0 to an increased value $(1+k)R_0$ over 5 seconds, and to hold the peak resistance for 15 seconds. The process was repeated for values $k = 0.15, 0.16, 0.17$, and 0.18 for the larger tube and for $k = 0.16, 0.17$, and 0.18 for the smaller tube. The tubes are shown after shape setting and cleaning in Figure 6(c), with the resulting total bending angles indicated, which turned out slightly less than the desired bending angle of $90°$. The resulting precurvatures are listed in Table 1.

A manual actuation setup, shown in Figure 7, was constructed to measure the distal angle of our modified tubes over a range of input angles. Rotary stages (Optics Focus MAR-60L-P) were used to provide independent rotation of the inner and outer tubes. The inner tube was connected to its rotary stage by a larger rigid steel tube, such that the effective straight transmission length of the inner tube was only 21 mm behind the base of the outer tube. A graduated disk and pointer were used to measure the output angle of the tube pair. The graduated disk has angular increments of $1°$ and is attached to the outer tube while the pointer is attached to the inner tube.

We rotated the tubes by equal angles in opposite directions in $5°$ increments (resulting in $10°$ increments in $\psi_2(\beta_2) - \psi_1(\beta_1)$ from $0°$ to $360°$. At each configuration, we performed a small insertion/retraction motion of the inner tube using a linear stage (Optics Focus MDX-4090-60) to eliminate frictional effects, as discussed in [40].

B. Results

We generated model-predicted input-output angle curves for the unmodified and modified tube pairs by solving our general model equations numerically, with boundary conditions accounting for additional transmission torsion in the straight length of the inner tube. The results are shown in Figure 8, along with the data from the experimental measurements on the modified tubes (red dots). The only calibrated parameter in this dataset is the initial relative angle of the tubes since

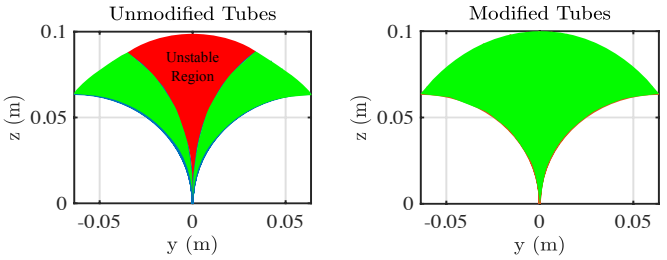

Figure 9. The y-z view of the subset of the workspace generated by rotating the tube bases equal amounts in opposite directions. Green shaded areas indicate stable regions in the workspace while red indicates unstable regions.

this is difficult to set precisely. The plot shows good agreement between the model and the data with an RMS error of $1.8°$ and a max error of $15°$, occurring at approximately $120°$ and $240°$. The error pattern indicates that the cut tubes have slightly more anisotropy than the intended design.

A view of the workspace perpendicular to the y-z plane is shown in Figure 9. The full model of Section II is solved to obtain the robot shape in space as the tubes are rotated by equal increments in opposite directions such that $\psi_2(\beta_2) - \psi_1(\beta_1)$ ranges from $0°$ to $360°$. When $\psi_2(\beta_2) - \psi_1(\beta_1) = 0$, the precurved tube shapes lie entirely in the y-z plane, and as they are counter-rotated, the stiffness-balanced pair straightens and then curves towards the opposite side. Note that while the unmodified pair snaps across the gap, the modified tube pair never snaps and has a more evenly distributed set of configurations with respect to uniform changes in $\psi_2(\beta_2) - \psi_1(\beta_1)$.

V. Conclusions

Concentric tube robots have excited researchers as some of the most slender robots for applications in confined, tortuous spaces. However, the unstable "snapping" problem can frustrate their practical application, since it creates limitations on how curved the robots can be and presents a serious safety hazard in many surgical contexts. Using a model that captures transverse anisotropy, we have presented a fundamentally new understanding of the problem, revealing that selectively reducing the rigidity of the tubes only about the axis of precurvature has a strikingly beneficial effect on the rotational stability of concentric tube robots. A major added benefit of this new insight is that the total reduction in the robot's stiffness is much less than previous approaches to improving stability through modification of the tube's structural rigidity. The new approach was validated experimentally with a pair of highly curved tubes that would have exhibited snapping behavior if not for their structural modification. This new insight into concentric tube robots will substantially expand their capability, opening the door to future applications with highly curved robots.

References

[1] H. B. Gilbert, D. C. Rucker, and R. J. Webster III, *Concentric Tube Robots: The State of the Art and Future Directions*. Springer International Publishing, 2016, pp. 253–269.

[2] R. J. Webster, III, J. M. Romano, and N. J. Cowan, "Mechanics of Precurved-Tube Continuum Robots," *IEEE Transactions on Robotics*, vol. 25, no. 1, pp. 67–78, 2009.

[3] D. C. Rucker, R. J. Webster, G. S. Chirikjian, and N. J. Cowan, "Equilibrium Conformations of Concentric-tube Continuum Robots," *The International Journal of Robotics Research*, vol. 29, no. 10, pp. 1263–1280, apr 2010.

[4] P. E. Dupont, J. Lock, B. Itkowitz, and E. Butler., "Design and Control of Concentric-Tube Robots," *IEEE Transactions on Robotics*, vol. 26, pp. 209–225, 2010.

[5] C. Bergeles and P. E. Dupont, "Planning stable paths for concentric tube robots," in *2013 IEEE/RSJ International Conference on Intelligent Robots and Systems*. IEEE, nov 2013, pp. 3077–3082.

[6] R. Xu, S. F. Atashzar, and R. V. Patel, "Kinematic instability in concentric-tube robots: Modeling and analysis," in *5th IEEE RAS/EMBS International Conference on Biomedical Robotics and Biomechatronics*. IEEE, aug 2014, pp. 163–168.

[7] J. Ha, F. C. Park, and P. E. Dupont, "Elastic Stability of Concentric Tube Robots Subject to External Loads," *IEEE Transactions on Biomedical Engineering*, vol. 63, no. 6, pp. 1116–1128, jun 2016.

[8] H. Gilbert, R. Hendrick, R. Webster, and R. Webster, "Elastic Stability of Concentric Tube Robots: A Stability Measure and Design Test," *IEEE Transactions on Robotics*, vol. 32, no. 1, 2016.

[9] J. Till, V. Aloi, K. E. Riojas, P. L. Anderson, R. J. Webster III, and C. Rucker, "A dynamic model for concentric tube robots," *IEEE Transactions on Robotics*, vol. 36, no. 6, pp. 1704–1718, 2020.

[10] K. E. Riojas, R. J. Hendrick, and R. J. Webster, "Can elastic instability be beneficial in concentric tube robots?" *IEEE Robotics and Automation Letters*, vol. 3, no. 3, pp. 1624–1630, 2018.

[11] K. Leibrandt, C. Bergeles, and G. Yang, "On-line collision-free inverse kinematics with frictional active constraints for effective control of unstable concentric tube robots," in *2015 IEEE/RSJ International Conference on Intelligent Robots and Systems (IROS)*, 2015, pp. 3797–3804.

[12] M. Khadem, J. O'Neill, Z. Mitros, L. d. Cruz, and C. Bergeles, "Autonomous steering of concentric tube robots for enhanced force/velocity manipulability," in *2019 IEEE/RSJ International Conference on Intelligent Robots and Systems (IROS)*, 2019, pp. 2197–2204.

[13] C. Girerd, K. Rabenorosoa, P. Rougeot, and P. Renaud, "Towards optical biopsy of olfactory cells using concentric tube robots with follow-the-leader deployment," in *2017 IEEE/RSJ International Conference on Intelligent Robots and Systems (IROS)*, 2017, pp. 5661–5887.

[14] M. Khadem, J. O'Neill, Z. Mitros, L. da Cruz, and C. Bergeles, "Autonomous steering of concentric tube robots via nonlinear model predictive control," *IEEE Transactions on Robotics*, vol. 36, no. 5, pp. 1595–1602, 2020.

[15] C. Girerd, A. V. Kudryavtsev, P. Rougeot, P. Renaud, K. Rabenorosoa, and B. Tamadazte, "Slam-based follow-the-leader deployment of concentric tube robots," *IEEE Robotics and Automation Letters*, vol. 5, no. 2, pp. 548–555, 2020.

[16] T. L. Bruns, A. A. Remirez, M. A. Emerson, R. A. Lathrop, A. W. Mahoney, H. B. Gilbert, C. L. Liu, P. T. Russell, R. F. Labadie, K. D. Weaver, and I. Robert J. Webster, "A modular, multi-arm concentric tube robot system with application to transnasal surgery for orbital tumors," *The International Journal of Robotics Research*, vol. 40, no. 2-3, pp. 521–533, 2021.

[17] J. Ha, F. C. Park, and P. E. Dupont, "Achieving elastic stability of concentric tube robots through optimization of tube precurvature," in *2014 IEEE/RSJ International Conference on Intelligent Robots and Systems*. IEEE, sep 2014, pp. 864–870.

[18] R. J. Hendrick, H. B. Gilbert, and R. J. Webster, "Designing snap-free concentric tube robots: A local bifurcation approach," in *2015 IEEE International Conference on Robotics and Automation (ICRA)*. IEEE, may 2015, pp. 2256–2263.

[19] M. Boushaki, C. Liu, B. Herman, V. Trevillot, M. Akkari, and P. Poignet, "Optimization of concentric-tube robot design for deep anterior brain tumor surgery," in *2016 14th International Conference on Control, Automation, Robotics and Vision (ICARCV)*, 2016, pp. 1–6.

[20] J. Ha and P. E. Dupont, "Designing Stable Concentric Tube Robots Using Piecewise Straight Tubes," *IEEE Robotics and Automation Letters*, vol. 2, no. 1, pp. 298–304, jan 2017.

[21] J. Ha, F. C. Park, and P. E. Dupont, "Optimizing tube precurvature to enhance the elastic stability of concentric tube robots," *IEEE Transactions on Robotics*, vol. 33, no. 1, pp. 22–37, 2017.

[22] D. C. Rucker, B. A. Jones, and R. J. Webster III, "A Geometrically Exact Model for Externally Loaded Concentric-Tube Continuum Robots," *IEEE Transactions on Robotics*, vol. 26, pp. 769–780, 2010.

[23] J. Kim, D. Lee, K. Kim, S. Kang, and K. Cho, "Toward a solution to the snapping problem in a concentric-tube continuum robot: Grooved tubes

with anisotropy," in *2014 IEEE International Conference on Robotics and Automation (ICRA)*, 2014, pp. 5871–5876.

[24] H. Azimian, P. Francis, T. Looi, and J. Drake, "Structurally-redesigned concentric-tube manipulators with improved stability," in *2014 IEEE/RSJ International Conference on Intelligent Robots and Systems*. IEEE, sep 2014, pp. 2030–2035.

[25] D.-Y. Lee, J. Kim, J.-S. Kim, C. Baek, G. Noh, D.-N. Kim, K. Kim, S. Kang, and K.-J. Cho, "Anisotropic Patterning to Reduce Instability of Concentric-Tube Robots," *IEEE Transactions on Robotics*, vol. 31, no. 6, pp. 1311–1323, dec 2015.

[26] C. Girerd, T. Schlinquer, N. Andreff, P. Renaud, and K. Rabenorosoa, "Design of Concentric Tube Robots Using Tube Patterning for Follow-The-Leader Deployment," *Journal of Mechanisms and Robotics*, vol. 13, no. 1, 08 2020, 011006.

[27] K. A. Xin Jue Luo, T. Looi, S. Sabetian, and J. Drake, "Designing concentric tube manipulators for stability using topology optimization," in *2018 IEEE/RSJ International Conference on Intelligent Robots and Systems (IROS)*, 2018, pp. 1764–1769.

[28] J. A. Childs and C. Rucker, "Concentric precurved bellows: New bending actuators for soft robots," *IEEE Robotics and Automation Letters*, vol. 5, no. 2, pp. 1215–1222, 2020.

[29] S. Chen, R. Karthikeyan, and S. C. Ryu, "Towards the design of mechanically superior tubular structures for microcatheters," *Smart Materials and Structures*, vol. 28, no. 3, p. 035032, feb 2019.

[30] J. M. Hur, D.-S. Seo, K. Kim, J. K. Lee, K. J. Lee, Y. Y. Kim, and D.-N. Kim, "Harnessing distinct deformation modes of auxetic patterns for stiffness design of tubular structures," *Materials & Design*, vol. 198, p. 109376, 2021.

[31] S. S. Antman, *Nonlinear Problems of Elasticity*, 2nd ed., S. S. Antman, J. E. Marsden, and L. Sirovich, Eds. Springer Science, 2005.

[32] M. D. M. Kutzer, S. M. Segreti, C. Y. Brown, M. Armand, R. H. Taylor, and S. C. Mears, "Design of a new cable-driven manipulator with a large open lumen: Preliminary applications in the minimally-invasive removal of osteolysis," in *2011 IEEE International Conference on Robotics and Automation*, 2011, pp. 2913–2920.

[33] J. Kim, W. Lee, S. Kang, K. Cho, and C. Kim, "A needlescopic wrist mechanism with articulated motion and kinematic tractability for micro laparoscopic surgery," *IEEE/ASME Transactions on Mechatronics*, vol. 25, no. 1, pp. 229–238, 2020.

[34] J. Kim, W. Choi, S. Kang, C. Kim, and K. Cho, "Continuously variable stiffness mechanism using nonuniform patterns on coaxial tubes for continuum microsurgical robot," *IEEE Transactions on Robotics*, vol. 35, no. 6, pp. 1475–1487, 2019.

[35] S. Park, J. Kim, C. Kim, K.-J. Cho, and G. Noh, "Design optimization of asymmetric patterns for variable stiffness of continuum tubular robots," *IEEE Transactions on Industrial Electronics*, pp. 1–1, 2021.

[36] R. M. Murray, Z. Li, and S. S. Sastry, *A Mathematical Introduction to Robotic Manipulation*. Boca Raton, FL: CRC Press, 1994.

[37] D. Rucker and R. Webster III, "Parsimonious Evaluation of Concentric-Tube Continuum Robot Equilibrium Conformation," *IEEE Transactions on Biomedical Engineering*, vol. 56, no. 9, pp. 2308–2311, sep 2009.

[38] J. Till and D. C. Rucker, "Elastic stability of cosserat rods and parallel continuum robots," *IEEE Transactions on Robotics*, vol. 33, no. 3, pp. 718–733, 2017.

[39] H. Gilbert, R. Webster, R. Webster, and R. Webster, "Rapid, Reliable Shape Setting of Superelastic Nitinol for Prototyping Robots," *IEEE Robotics and Automation Letters*, vol. 1, no. 1, 2016.

[40] J. Ha, G. Fagogenis, and P. E. Dupont, "Modeling tube clearance and bounding the effect of friction in concentric tube robot kinematics," *IEEE Transactions on Robotics*, vol. 35, no. 2, pp. 353–370, 2019.